Jour. Fac. Sci., Hokkaido Univ., Ser. VII (Geophysics), Vol. 10, No. 1, 107-133, 1996.

Doppler Radar Observations on the Structure and Characteristics of Tropical Clouds during the TOGA-COARE IOP in Manus, Papua New Guinea — Characteristics of Cloud Clusters Analyzed with Doppler Radar and GMS-IR Data —

Osamu Kikuchi* and Hiroshi Uyeda

Division of Earth and Planetary Sciences, Graduate School of Science, Hokkaido University, Sapporo 060, Japan

(Received December 11, 1995)

Abstract

Two characteristic cloud clusters (24 Nov. and 21 Dec. 1992) during the observation period of TOGA-COARE IOP in Manus were chosen for analyses. In the time variation of radar-estimated rain rate, two modal distributions of large rain rate were recognized for convective portion. The first mode consisted of heavy rainfall in a convective cores of mature stage. The second mode corresponded to the relatively weak rainfall below the melting layer at the beginning of the dissipating stage. On the other hand, the predominance of a stratiform area and rainfall amounts relative to convective components through the lifetime of a cloud cluster was analyzed with radar data, even in the development to the mature stage of the cluster.

The analyses of GMS-IR data were combined with the rader data analyses in order to better understand the characteristics of cloud clusters. The extension of cloud area analyzed with GMS-IR data showed a time lag (a few hours) behind the evolution of the radar echo top height and echo area.

The existence of thick snow and/or ice layer above the melting layer in cloud clusters was supported by the comparison between the analyses of Doppler radar data and the analyses of GMS-IR data using the CST (Convective Stratiform Technique), which is the method to distinguish between convective and stratiform components of cloud clusters. The area and rainfall amounts determined from the CST did not agree with those observed and estimated using radars, when independent convection from a convection below the melting layer was recognized above the melting layer. Though the expansion of the low T_{BB} region caused a difficulty in the estimation of surface rainfall amounts from GMS-IR data, the extension of the low T_{BB} after the mature stage is considered as one of characteristics of cloud clusters in the equatorial west Pacific.

* Present Affiliation: Japan Air System, Haneda Airport, Tokyo 144, Japan.

1. Introduction

It is known that heat sources in the tropics play an important role in general circulations of the global atmosphere. In particular, the region around Papua New Guinea belongs to part of the "maritime continent", which is the name given by Ramage (1968) to the highly convective region comprised of the islands, peninsulas, and intervening seas of Indonesia, Malaysia, northern Australia, and Papua New Guinea. As pointed out by Ramage (1968), the latent heat released in clouds and precipitation over this tropical ocean warm water pool constitutes one of the primary sources of energy for the atmosphere. In order to reach some goals described in the TOGA COARE science plan WCRP (1989), which was mainly developed to reveal the interaction between the tropical atmosphere and the warm water pool, it is very important to understand the organization of convection in such phenomena as a cloud cluster and further, a super cloud cluster (Hayashi and Sumi (1986)). The reason for this is that global circulation is sensitive to rainfall distribution and the heating of the large-scale environment by deep convection as shown by Hartmann et al. (1984) and DeMaria (1985).

In order to better understand the precise structures and characteristics of multi-scale convective systems (Nakazawa, 1988) within the TOGA COARE region, the combination of radar and satellite observations is required. Since most of the studies concerning multi-scale convective systems within the equatorial western Pacific region have been discussed only from satellite data, the understanding of the internal structure of multi-scale convective systems below the large cold cloud shields has not progressed. On the contrary, initial studies of the meso-scale structure of tropical convection were carried out during GATE (Global Atmospheric Research Program's Atlantic Tropical Experiment) by Houze and Betts (1981) and others. However, the study using both radar and satellite, which focuses on the understanding of multi-scale convective systems, wasn't done during GATE.

Adler and Negri (1988) have proposed a technique that uses GMS (Geostationary Meteorological Satellite) infrared (IR) data to distinguish between convective components and stratiform components of meso-scale convective systems. This technique offers the possibility of understanding the movement of cloud clusters and determining their convective and stratiform components such as area and rainfall amounts over regions not covered by surface-based radar. Goldenberg et al. (1990) applied this technique to a large cloud cluster over the South China Sea during the Winter Monsoon Experiment (WMONEX).

They showed good conformance in their application of this technique. In this paper, this technique was applied around our radar observation site. The comparison between radar results and results obtained from this technique using GMS-IR data enabled us to reveal the characteristics of cloud clusters.

TOGA COARE IOP (Intensive Observation Period) was chosen from November, 1992 to February, 1993 to maximize the probability of observing strong westerly wind events, which is the most intense air-sea interaction. We carried out ground-based dual-Doppler observations using two X-band Doppler radars on Manus Island (2.0°S, 147.2°E), Papua New Guinea, frm 15 November 1992 to 20 January 1993. Of some cloud clusters observed using Doppler radars during TOGA COARE IOP, three characteristic cloud clusters were chosen and analyzed using the method of identifying convective and stratiform components of meso-scale convective systems from GMS-IR data in comparison with radar results in order to reveal the characteristics of cloud clusters.

This paper presents the characteristics of cloud clusters over the equatorial western Pacific ocean from the dual-Doppler analysis, and an evaluation of convective and stratiform components of cloud clusters determined from GMS-IR data relative to that determined from Doppler rader data.

2. Data

The radar data obtained during the observation period in Manus (Uyeda et al., 1995) was utilized for the analysis. Single Doppler radar by the name of HUML (Meteorological Laboratory, Hokkaido University) placed at Nabu (see Fig. 2 of Uyeda et al. (1995)) was utilized for PPI and RHI analyses. Dual-Doppler radar analysis was also carried out to obtain the information on wind fields in clouds. The other Doppler radar is ILST (Institute of Low Temperature Science, Hokkaido University) placed at Momote (see Fig. 2 of Uyeda et al. (1995)). Specifications and locations of the two radars are described by Uyeda et al. (1995).

The satellite data set used in this study is the TOGA-COARE hourly infrared (IR) satellite data set throughout the TOGA-COARE IOP in CD-ROM (provided by Nakazawa, Meteorological Research Institute, Japan Meteorological Agency) from the Japanese Geostationary Meteorological Satellite (GMS). The resolution of the GMS-IR data is $0.1^\circ \times 0.1^\circ$ corresponding to about 10 km × 10 km. The spatial coverage is from 130°E to 180°E in longitude and from 15°N to 15°S in latitude. In addition to this data, the GMS-IR data of $0.05^\circ \times 0.05^\circ$ mesh data corresponding to about 5 km × 5 km was used in order to find the

structure and characteristics of cloud clusters in detail. The spatial coverage is from 140°E to 160°E in longitude and from 5°N to 10°S in latitude. They contain mesh data in the form of equivalent black body temperature (T_{BB}). The temperature resolution is 1° K in both sets of data.

3. Method

3.1 Convective Stratiform Technique (CST)

a) Outline of the method

In analyzing the GMS-IR data, we followed the basic CST algorithm of Adler and Negri (1988), henceforth referred to as AN. Goldenberg et al. (1990), henceforth referred to as GHC, modified the empirical "discrimination line" of AN for their application, because the cold cloud top temperatures in the WMONEX region were typically 15 to 20°K lower than that of the second Florida Area Cumulus Experiment (FACE) data examined by AN. The same discrimination line of WMONEX case applied by GHC was used in this analysis, because the WMONEX domain is located in a part of the maritime continent same as the TOGA-COARE domain. The CST is a technique to distinguish between convective components and stratiform components of meso-scale convective cloud systems that have extensive cirroform tops using satellite IR data. The CST determines the convective portion from the local T_{BB} minima referring their T_{BB} slope. The convective area and rain rate is estimated from the value of the relative minimum T_{BB}. The stratiform portion is determined by a modal T_{BB} around convective cores in the mature stage. The details are described in the following section.

b) Location of convective cores in the IR imagery

The first step in the CST is to distinguish convective cores. To accomplish this, each satellite data is analyzed independently. The GMS-IR brightness temperature (T_{BB}) field is searched for local T_{BB} minima ($T_{\min}$) in a 50 km×50 km square centered at $T_{\min}$. If the minima encompasses more than one IR pixel, the location of the pixel with the largest "slope parameter" (S) is used. In this application of the CST, however, we focus on only the convective core with a higher cloud top. Toward this aim, the threshold temperature of the locating convective core is decided from the comparison with radar echo patterns for each case presented in this paper. In Case 1, the threshold of 215°K was selected. In Case 2 and 3, it was decided as 200°K. Next, in order to remove minima that represent thin, nonprecipitating cirrus, a slope parameter was calculated for each $T_{\min}$. The slope parameter used in this study is given by :

$$S=k(T_{i-1,j}+T_{i+1,j}+T_{i,j-1}+T_{i,j+1}-4T_{i,j}), \quad (1)$$

where i, j refers to the position of the pixel in the east-west and north-sorth direction for which S is calculated, respectively. The factor k is multiplied to be equivalent to the AN slope parameter. For 0.05° and 0.1° resolution data, $k=0.290$ and $k=0.145$, respectively.

The pairs of $T_{\min}$ and S calculated above were then compared with an empirical discrimination line to distinguish whether each $T_{\min}$ is associated with convective core or not. According to GHC, the pixel of $T_{\min}$ is expected to indicate the location of a convective core if

$$S \geq \exp[0.0826(T_{\min}-207)]. \quad (2)$$

This relationship shows that a large slope implies a more clearly defined minimum than does a small slope, since the small slope indicates the weak gradients associated with cirrus.

c) Estimation of convective precipitation area and rain rate

The next step in the CST is to assign areal coverage of convective precipitation (A_c (km^2)) and the average convective rain rate (R_c (kgm^{-2} h^{-1})) to each of the cores selected through the screening process described in Sec. 3.1b). AN and GHC used the result from a one-dimensional cumulus model by Adler and Mack (1984) to assign them. In order to compare GMS-derived temperatures with the result from a one-dimensional model, the difference in scale must be resolved. The correction is given by

$$T_{\min}-T_c(\mathrm{K})=\begin{cases}0.283T_{\min}-56.6, & (T_{\min}>200\mathrm{K})\\ 0, & (T_{\min}\leq 200\mathrm{K}).\end{cases} \quad (3)$$

where T_c is the corrected temperature.

According to GHC, in order to obtain an estimate of the average rain rate R_{ci} (mmh^{-1}) in the area A_{ci} (km^2) associated with the i-th core, the linear relationship of $\ln(A_{ci})$ and $\ln(R_{ci})$ to the cloud-top temperature of the i-th convective core can be written

$$\ln(A_{ci})=aT_{ci}+b, \quad (4)$$
$$\ln(R_{ci})=cT_{ci}+d, \quad (5)$$

where a, b, c and d are constants. The index i refers to the i-th core. In this analysis, We used the value of $a=-0.0492$, $b=15.27$, $c=-0.0157$, and $d=4.76$ same as GHC applied in WMONEX.

d) Area covered by stratiform precipitation

For a T_{BB} threshold, T_S, is used to identify the stratiform precipitation

areas. Since this threshold should coincide with the relatively thick portion of mature anvils, the modal T_{BB} (T_{mode}) in the frequency distribution of anvil T_{BB} was sought as an indicator of the anvil background temperature.

As the first procedure, the T_{mode} in 80 km×80 km box, centered on each convective center for which $S \leq 4.0$, was determined. A cutoff value of S was selected empirically by AN to exclude the young, growing convective cells which normally have larger slopes than the mature systems with extensive cirroform anvils. The weighted mean of all of the modal temperature for that image is given as:

$$\overline{T_{\mathrm{mode}}} = \frac{\sum_i W_i T_{\mathrm{mode}(i)}}{\sum_i W_i}, \tag{6}$$

where $T_{\mathrm{mode}(i)}$ is the mode temperature for the i-th convective cell and W_i the number of pixels in the box surrounding that cell for which $T_{BB} = T_{\mathrm{mode}(i)}$.

According to GHC, the threshold of the area covered by stratiform precipitation, T_S, is given as

$$T_S(\mathrm{K}) = \overline{T_{\mathrm{mode}}} + x, \tag{7}$$

where $x = 7$°K. GHC showed better conformance in their application for tropical meso-scale convective cloud systems using this relationship rather than the $T_S = T_{\mathrm{mode}}$ equation used by AN.

e) Assignmnt of stratiform rain rate

The next step in applying the CST is to assign rain rates to the stratiform regions bounded by T_S. The method used by AN and GHC was to assign a nominal rain rate of 2 kg m^{-2} h^{-1} to the pixels classified by the technique as a stratiform region. However, the area-integrated rain rate calculated from the rain rate in AN and GHC was much larger than the HUML radar-derived area-integrated rain rate which is calculated using the Z-R relationship derived by Marshall and Palmer (1948) given by

$$Z = 200R^{1.6}, \tag{8}$$

where Z is the radar reflectivity factor in mm^6 m^{-3}, and R is rainfall rate in kg m^{-2} h^{-1}. From the comparison with radar data, we assigned 0.5 kg m^{-2} h^{-1} as the stratiform rain rate.

3.2 Dual-Doppler analysis

For the analysis of the wind field within the cloud analyzed with the GMS-IR data, a dual-Doppler analyses were performed utilizing data set of the two Doppler radars placed on Manus Island. The algorism of dual-Doppler radar

data analyses was that provided by Satoh (see Satoh et al. (1995) about the details of the analysis method).

The data obtained by two Doppler radars on the spherical polar coordinates was interpolated to 120 km×120 km Cartesian grids. Grid spacings used were 1 km in the horizontal and 0.5 km in the vertical without 0.25 km at the lowest boundary of the vertical grid. The vertical motion was determined by the upward integration of the anelastic equation of mass continuity. For each vertical colums, zero vertical velocity was assumed to occur at 0.25 km in height at the lower boundary. In this analysis, the relaxation method using the continuity equation was used to give a consistent field of horizontal velocities and diver-gence with a maximum error potential in w of 0.1 ms^{-1}.

4. Case studies

4.1 Case 1 (24 November, 1992)

A Part of a cloud cluster was observed using Doppler radars throughout its lifetime from the developing to the dissipating stage on November 24, 1992. The characteristics of this cloud cluster were analyzed using radar and GMS-IR data.

Figure 1 shows the time-longitude section of three-hourly GMS-IR images between the equator and 5°S from 19LST (Local Standard Time in Manus Island, Papua New Guinea)[1] on November 23 to 01LST on November 25. From 01LST on November 24, the cloud clusters of 500 km in horizontal scale existed in the eastern and the western side of Manus Island. However, we can see no clouds around Manus Island up to 07LST. From 10LST, cumulus convection seemed to be active around Manus Island, forming part of the western end of a new cloud cluster near Manus Island. The cloud cluster on the western side moved north-westward. At 16LST, it appeared that the cloud area around Manus Island reached its maximum. According to the mean flow pattern of GANAL (Global Analysis by the Japan Meteorological Agency) at 200hPa level (not shown), an easterly flow associated with the anticyclonic circulation over northern Australia existed over Manus Island at 10LST on Novmber 24. The wind field of GANAL at 850hPa also showed the easterly trade winds over Manus Island and the existnce of eddy along the equator to the north of Manus Island. The westerlies were not seen during the cloud cover over Manus Island on 24 November. Six-hourly sounding wind data (see Fig. 3 of Uyeda et al.

[1] LST=UTC+10 (hour)

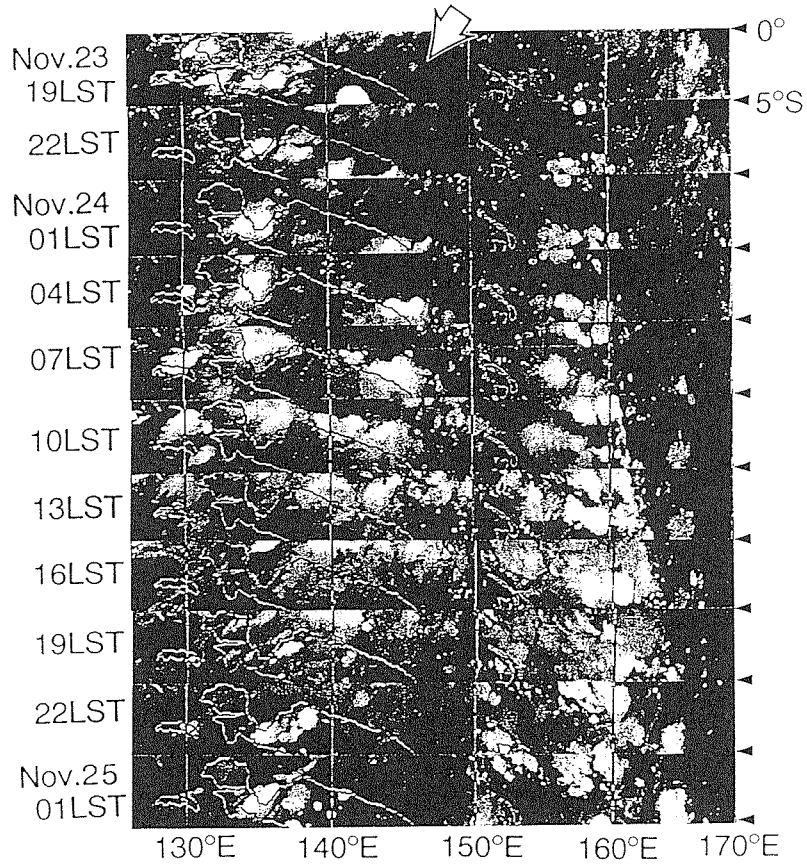

Fig. 1. Time-longitude section of three-hourly GMS-IR images between the equator and 5°S from 19LST on November 23 to 01LST on December 25, 1992. The tip of white arrow indicates the location of Manus Island (2.0°S, 147.2°E), Papua New Guinea. The location of HUML radar site is shown by (+) mark on the image of 13LST and 16LST.

(1995)) on November 24 also supported the predominance of an easterly wind through the troposphere.

The meso-scale structure and evolution of a part of the cloud cluster is shown as the radar echo patterns in Fig. 2. The time sequence of radar echoes of hourly PPI patterns at an elevation angle of 3° of reflectivity from 11LST to 16LST on November 24 is shown. From 11LST, some echoes were forming over Manus Island and the eastern ocean. At 12LST, eastern ehoes aligned from north to south, while echoes over Manus Island, which were observed frequently in the daytime during TOGA COARE IOP, were also developing.

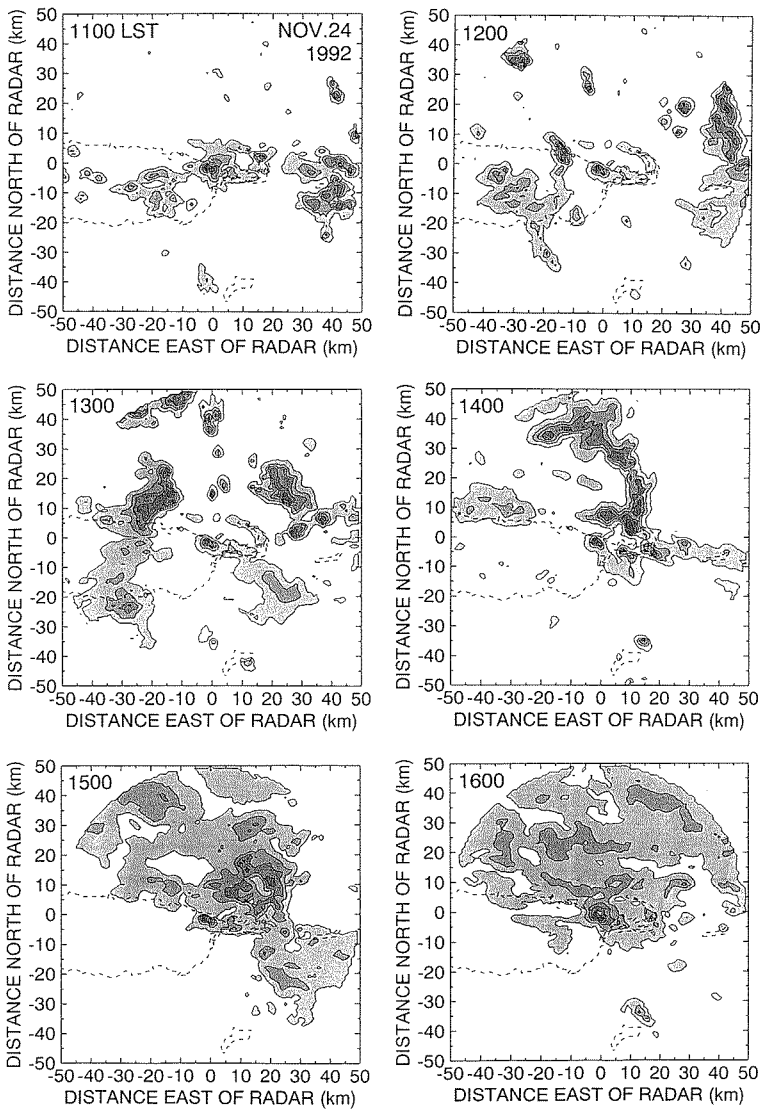

Fig. 2. The time sequence of radar echoes of hourly PPI patterns of reflectivity from 11LST to 16LST on November 24, 1992 by HUML radar. The elevation angle is 3° and the range covers a radius of 60 km. The reflectivity contour is 4dBZ interval starting from 19dBZ.

These developing echoes were intense with a maximum reflectivity near 40dBZ at 13LST. The PPI patterns suggest that this time (around 13LST) corresponds to the mature stage of this cloud system around Manus Island. At 14LST, eastern echoes and echoes over Manus Island were merging and forming a line shape. After 15LST, stratiform echoes (<22dBZ) were in domination and the northern part of radar range was mainly covered with stratiform echoes at 16LST. Therefore, it is suggested that the echoes at 15LST corresponds to the beginning of dissipating stage. This was supported by the decrease of updraft region (not shown) derived from dual-Doppler analysis. The vertical profile of the equivalent potential temperature also shows a convective overturning in between the 10LST and 16LST profiles (not shown). In this paper, the value of 22dBZ was used as a threshold reflectivity between convective and stratiform regions. The value of 22dBZ was chosen since the reflectivity of the echo area with large reflectivity and large gradient of reflectivity (convective portion) was mostly larger than 22dBZ and the reflectivity of wide spread weak echo (stratiform portion) was less than 22dBZ.

The characteristics of these structures are depicted in RHI patterns of velocity and reflectivity as shown in Fig. 3. We can obviously see the low level convergence and the middle to upper level strong divergence in Fig. 3(a); this

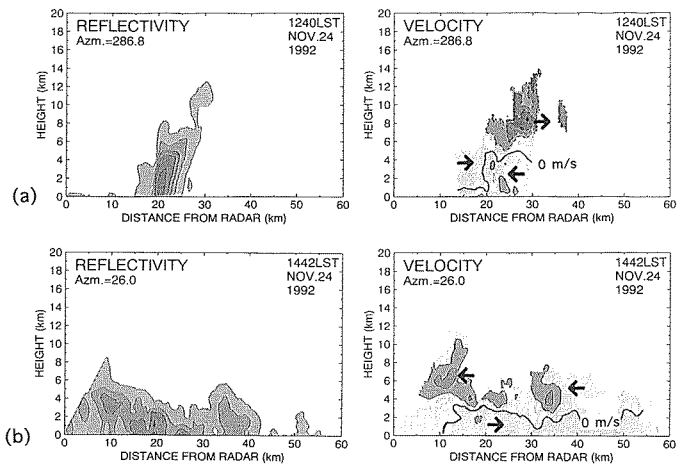

Fig. 3. The radar echoes of RHI scan of reflectivity and velocity at (a) 1240LST and (b) 1442LST on November 24. Reflectivity contours are the same as Fig. 2. Solid and dashed contours of velocity indicate component toward radar and away from radar respectively. Contour is every 4 m/s starting from 4 m/s. Thick solid line denotes the velocity component of 0 m/s. Direction of the volocity component is additionally shown by the arrow.

corresponds to the mature stage. The convective core was very intense, with about 40dBZ and the echo top over 19dBZ reached about 13 km. On the other hand, Fig. 3(b) shows the stratified velocity pattern, corresponding to the dissipating stage. Small horizontal gradient of velocity component without large convergence indicates the stratified radar echo feature. Though we can see some strong reflectivity portions in Fig. 3(b), they are shallower and weaker than those in Fig. 3(a) and also they exist below the melting layer at an altitude about 4.5 km.

In order to see the time evolution of clouds convective activity of clouds from radar data and cloud area from GMS-IR data are examined; the echo top

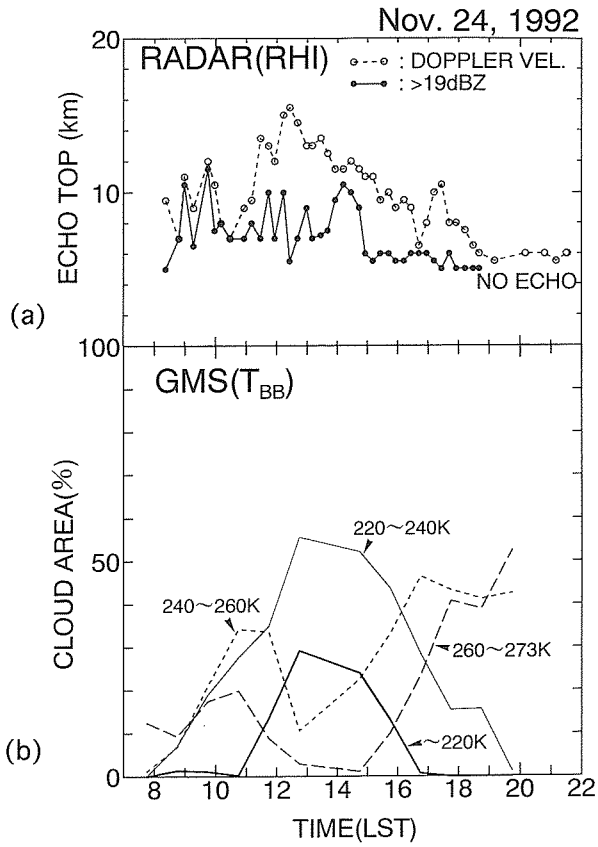

Fig. 4. (a) The radar echo top height of reflectivity over 19dBZ (solid circle) and the top height of the area where Doppler velocity is obtained (open circle). (b) Percentage contributions of cloud area by four T_{BB} thresholds to the radar coverage area.

height was compared with the percentage contributions of the cloud area classified by four T_{BB} thresholds within the radar coverage. The time evolution of the relations between the parameters is shown in Fig. 4. The echo top height was derived from the RHI of reflectivity over 19dBZ and additionally from that of Doppler velocity (from the area where Doppler volocity is obtained). Though the area where Doppler volocity is obtained depend on the distance from the radar, the area denotes the existence of precipitation particles. The data used as hourly GMS-IR data of 0.05° resolution, but unfortunately, the GMS-IR data at 14LST was missing. Figure 4 shows the development of cloud area and cloud height. Cloud area of T_{BB} from 200K to 240K and T_{BB} less than 200K increased rapidly (about 10%/hour) up to 12LST. A rapid increase in cloud area of T_{BB} below 240K, from 40% to 80%, is seen from 12LST to 13LST. The cloud area of T_{BB} below 240K, corresponding to the cloud top height over 10 km, reached over 80% from 13LST to 15LST. From 15LST to 17LST, the lower cloud (240-260K and 260-273K) area increased rapidly (about 15%/hour). On the other hand, the radar echo top abruptly rose and reached about 12 km of the echo top of Doppler velocity pattern at 1130LST. From 15LST, in spite of the large expansion of a higher cloud top from T_{BB} values at 15LST, stratiform lower echoes were dominating in the radar echo patterns. Both time evolutions of T_{BB} area and radar echo top show rough agreement. However, we see the time lag in this comparison between these time evolutions ; development of echo top height is ahead of that of T_{BB} cloud area.

Next, we tried to identify the convective and stratiform components of a cloud cluster using GMS-IR data. In order to accomplish this identification, the CST was utilized. The area of convective radar echo was small and narrow characteristically during TOGA-COARE radar observations. Moreover, since the gradient of T_{BB} must be calculated to determine the convective cores in the CST, the resolution of GMS-IR data used in the CST needed to be as high as possible. For this requirement, GMS-IR data of 0.05° resolution, which is the maximum rsolution possible, was used in the following analyses. The results of the CST at 13LST and 15LST using 0.05° resolution are shown in Fig. 5. The area where the CST was applied is 2° square centered at the HUML radar site. The time, 13LST and 15LST, corresponds to the convective period in the mature stage and the period of extension of stratiform echoes at the beginning of the dissipating stage, as identified from radar echo patterns, respectively. In addition to the result of the CST, the distribution of the radar echo top height over 19dBZ, derived from volume scans, is also shown in Fig. 5. Figure 5(a) shows good conformance of tall echo region with the location of convective

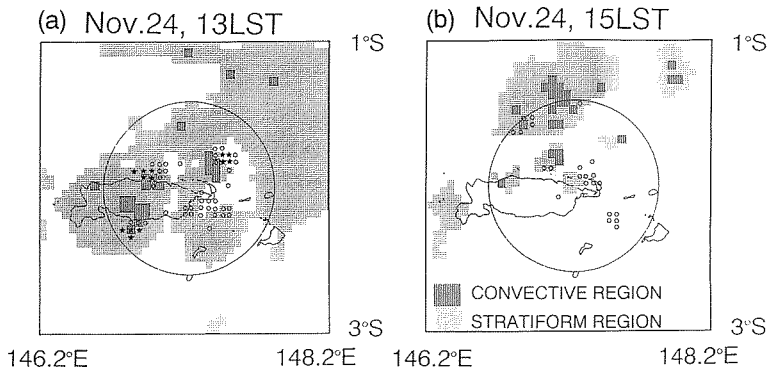

Fig. 5. CST-derived convective and stratiform regions using GMS-IR data of 0.05° resolution (a) at 13LST and (b) at 15LST on November 24, 1992. Light- and dark-shaded regions indicate stratiform and convective regions, respectively. The area is 2° square centered at HUML radar site. The radar echo (>19dBZ) top height of over 6 and 8 km are shown by the symbols of open circle and solid star respectively.

region determined from the CST over the eastern ocean and Manus Island at 13LST. In contrast, at 15LST as shown in Fig. 5(b), the CST-derived convective regions were seen within the low echo top region, where strong echoes were below the melting layer as shown in Fig. 2. These results derived from the comparison between the CST and radar show that it is difficult to obtain a good conformance between the CST pattern and the distribution of a radar echo top height at the dissipating stage. It is thought that this disagreement at the dissipating stage results from the fact that the method of the CST, which distinguishes the stratiform region from the T_{BB} distribution around convective cores at the mature stage, is not applicable to the dissipating stage.

In order to examine the possibility of rainfall estimation by the CST and the time evolution of relationships between the CST and radar echo, the area-integrated rain rates and rainfall amounts of convective and stratiform regions within the radar coverage are shown in Fig. 6 for the radar echo and the CST. In ths figure, the convective precipitation was calculated from the PPI (el.=3°) reflectivity data over 22dBZ using the Z-R relationship [Eq. (8)]. The stratiform precipitation was calculated from that of 19dBZ to 22dBZ. The curve of the convective rain rate estimated from the radar reaches its maximum at 13LST and shows the second peak at around 15LST. However, since the second peak in the convective rain rate estimated from radar is smaller than the first one, the type of rainfall is supposed to be different from heavy rainfall in

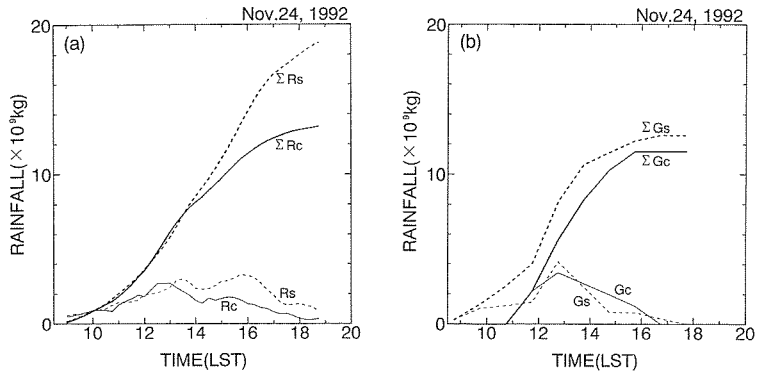

Fig. 6. Convective and stratiform area-integrated rain rates and time-integrated rainfall amounts within the radar coverage determined by (a) radar and (b) the CST. Convective rain rates (R_c) from radar are calculated for the reflectivity data over 22dBZ at an elevation angle of 3°. Stratiform rain rates (R_s) from radar are calculated for the reflectivity data from 19 to 22dBZ. Time-integrated radar-derived convective (ΣR_c) and stratiform (ΣR_s) rainfall amounts are shown by thick lines. The CST-derived convective and stratiform rain rates are denoted by G_c and G_s, respectively. The time-integrated CST-derived convective (ΣG_c) and stratiform (ΣG_s) rainfall amounts are shown by thick lines.

the mature stage. The period of the second peak corresponds to the stronger echo below the melting layer within the stratiform echo as shown in Fig. 3(b).

The curve of convective rain rate derived from the CST shows general conformance with that from the radar. On the other hand, the stratiform rain rate estimated from the radar reached its maximum in the dissipating stage due to a large coverage of stratiform echoes. However, stratiform area-intgrated rain rate was nearly as large as the convective area-integrated rain rate in the development to the mature stage. This implies that a stratiform region of CST grew around the convective core in the development to a mature stage of the cloud system same as that of radar echo parrerns. The relationship between the amounts of convective precipitation and those of stratiform precipitation also shows that both precipitation types are comparable even in their development to a mature stage in this cloud cluster. Though the curve of total rainfall estimated from radar shows nearly the same contribution of both convective and stratiform rainfall up to 14LST, stratiform rainfall is predominant in dissipating stage. In addition, in spite of the underestimation of stratiform rainfall derived from the CST in the dissipating stage, the stratiform rainfall exceeded convective rainfall throughout the lifetime of the cloud cluster. This implies

that the contribution of convective components is smaller than that of stratiform components in both areal coverage and amounts of precipitation.

4.2 Case 2 (21 December, 1992)

A prominent cloud cluster with a large coverage of a very low T_{BB} region in GMS-IR images was observed around Manus Island on December 21, 1992. In particular, the cloud area of T_{BB} below 220K, corresponded to the clound top height over about 12.5 km, occupying the whole area within the radar coverage from 13LST to 17LST. This cloud cluster was analyzed using the GMS-IR and radar data as in Case 1.

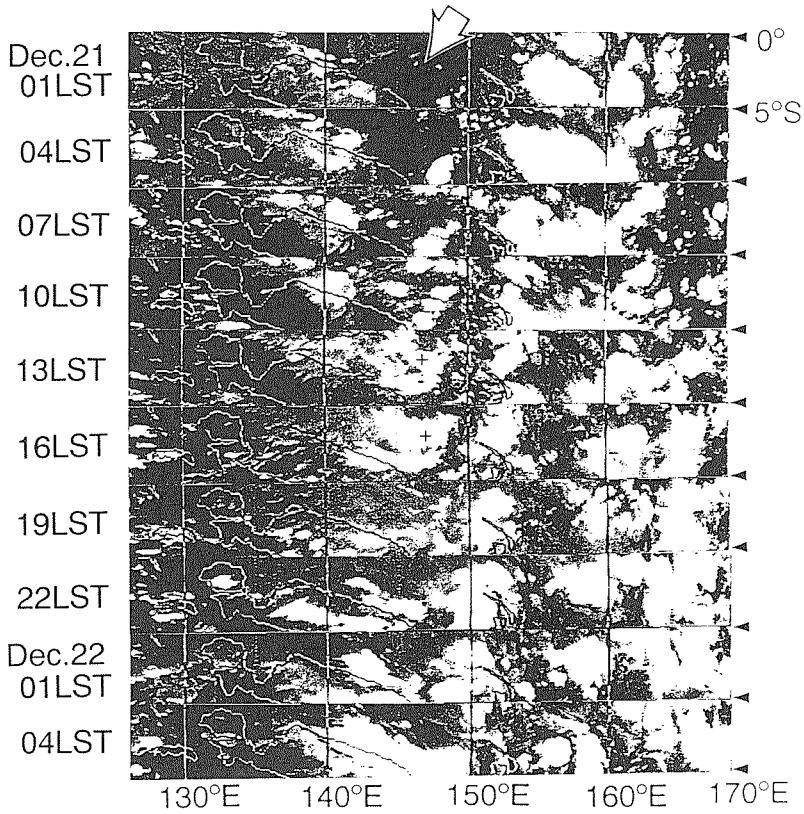

Fig. 7. Time-longitude section of three-hourly GMS-IR images between the quator and 5°S from 01LST on December 21 to 04LST on December 22, 1992. The tip of white arrow indicates the location of Manus Island (2.0°S, 147.2°E), Papua New Guinea. The location of HUML radar site is shown by (+) mark on the image of 13LST and 16LST.

Figure 7 shows the time-longitude section of three-hourly GMS-IR images between the equator and 5°S from 01LST on December 21 to 04LST on December 22. From 01LST on December 21, a cloud cluster of 200 km in horizontal scale moved north-westward slowly from the south-eastern side of Maus Island.

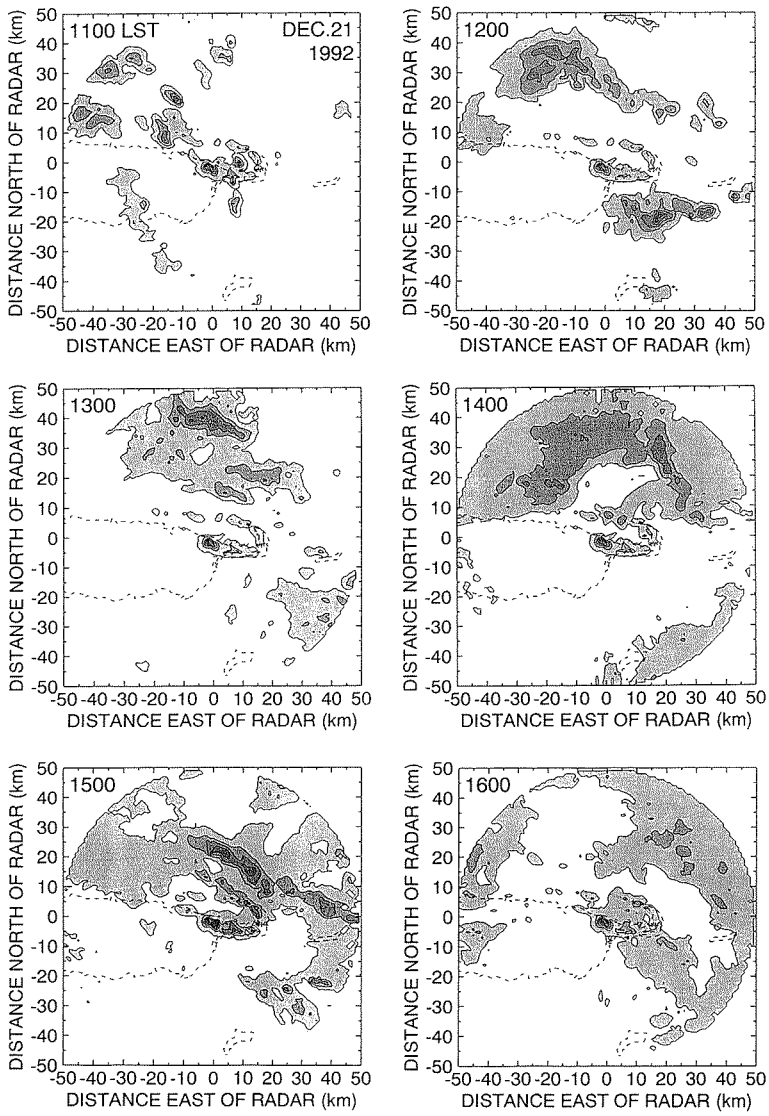

Fig. 8. Same as Fig. 2 except for the period from 11LST to 16LST on December 21, 1992.

On the other hand, we could see another cloud cluster of 200 km in the horizontal scale developing rapidly along 145°E at 10LST. At 13LST, these two cloud clusters seem to merge into a large cloud cluster of 500 km in horizontal scale over Manus Island. The cloud cluster seems to have had a very low cloud top temperature. At 19LST, it appears that the cloud cluster dissipated abruptly and moved westward slowly. After that, it appears that the outflow associated with the dissipation of this cloud cluster caused the formation of new cloud cluster along the main land of Papua New Guinea.

The mean flow pattern of this day shows an easterly flow in the upper troposphere and a westerly flow associated with cyclonic circulation in the eastern side of Manus Island in the lower troposphere. According to sounding data at Momote, the vertical wind shear was very large, at about $4\times10^{-3}\,s^{-1}$ between 500hPa and 900hPa. However, the convective instability in the lower troposphere was weaker in this case than in Case 1.

Figure 8 shows the time sequence of radar echoes of a part of the cloud cluster. These are hourly PPI patterns of reflectivity from 11LST to 16LST on December 21 at an elevation angle of 3°. From 11LST, some echoes were entering into radar coverage and were seen over Manus Island and the northwestern ocean of Manus Island. These northwestern echoes were moving eastward slowly and organized into a large echo at 12LST.

GMS-IR images in Fig. 7 shows the merger of two cloud clusters at 13LST, however radar echo patterns as shown in Fig. 8 show the extension of stratiform area around the organized stronger reflectivity echoes at 13LST. At 15LST, the organized echoes were aligned from northwest to southeast. However, almost all echoes around the line echo were occupied by weak stratiform echoes and low level updraft was weakened as will be shown in Fig. 10. After 16LST, the stratiform echoes moved eastward slowly. It appears that the time around 12LST corresponds to the mature stage and the period around 15LST corresponds to the dissipating stage of this cloud system around Manus Island from radar PPI patterns. RHI patterns around 12LST (not shown) also show a weak low level convergence and an upper level strong divergence ; this corresponds to the mature stage. However, the convective core was not so intense as that shown in Case 1 and the echo top height over 19dBZ reached only 9 km which was lower than that in Case 1 of 13 km. On the other hand, RHI patterns around 15LST, corresponding to the dissipating stage, showed a stratified velocity pattern and a weak bright band around the melting layer (4.5 km). The echo top height over 19dBZ was below 6 km and constant. In spite of this low echo top height, the area of T_{BB} below 220K in GMS-IR data occupied almost the

whole area within radar coverage from 13LST to 17LST. This opposite relationship, low radar echo top height and high cloud top altitude, implies the existence of a thick snow and ice layer above the radar's detectable echo top height.

The horizontal and vertical wind fields in this cloud cluster were calculated using dual-Doppler analysis. The ground-relative horizontal wind fields and the updraft region over 2 ms^{-1} at 12LST and 15LST derived from dual-Doppler analysis are shown in Fig. 9 and Fig. 10, respectively. The general flow at an altitude of 1.0 km was from westerly to northwesterly at both times. At the 5.0

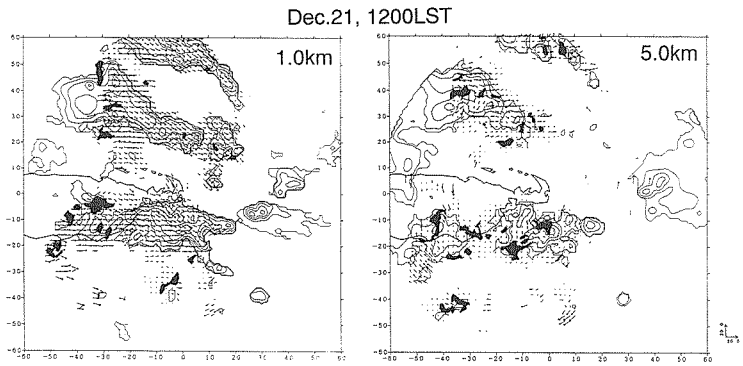

Fig. 9. Wind field at the 1.0 km and 5.0 km heights derived from dual-Doppler analysis superimposed on the horizontal maps showing the radar reflectivity (dBZ) at 5dBZ intervals from 15dBZ and ground-relative horizontal vector winds at 12LST on December 21. Reflectivity is that of ILTS. Black region indicates updraft region over 2 ms^{-1}.

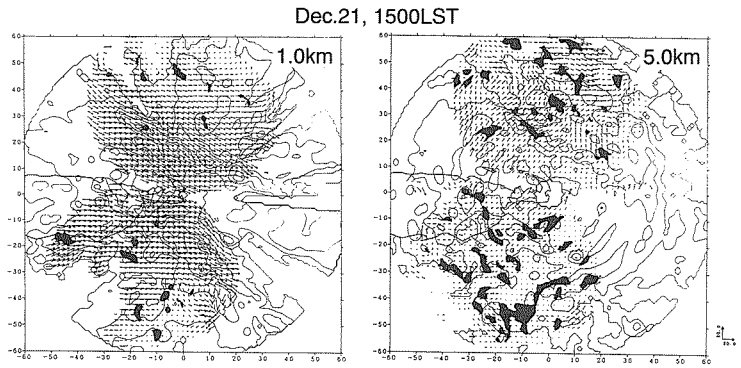

Fig. 10. Same as Fig. 9 except for the time of 15LST on December 21.

km level, in spite of the expansion of a stratiform echo, the horizontal wind field was not uniform at 15LST. The area of updraft region at 1.0 km level is comparable with that at 5.0 km level at 12LST in the mature stage. On the other hand, though a low level updraft was not apparent, the increase of updraft region at 5.0 km, over melting layer, was found at 15LST within the dissipating stage. The differences in the vertical motion fields between below and over the melting layer at two different times suggest different mechanisms of making vertical motion. This difference was also seen in Case 1 (not shown).

The results of the CST at 13LST and 15LST using GMS-IR data of 0.05° resolution are shown in Fig. 11 with the distribution of radar echo top height over 19dBZ. Since the GMS-IR data at 11LST and 12LST was missing, 13LST data of GMS-IR, which corresponds to the nearest time to the mature stage, was utilized for CST analysis. And 15LST corresponds to the period of extension of the stratiform echoes at the dissipating stage, which was identified from radar echo patterns, as shown in Fig. 8. Through almost the whole area was occupied by radar echoes with echo top heights (>19dBZ) from 4 km to 6 km at both times, relatively large region of CST-derived convective component were seen in some places at both times. It is thought that these results were caused by the lower T_{BB} values associated with an overspread thick snow and ice layer in the upper troposphere. The believed existence of this snow and ice layer is supported by a vertical cross section (along the line A-A′ in Fig. 11) shown in Fig. 12. This shows that the height of velocity detectable portion and the existence of an upward motion are a few kilometers above the echo top (greater than 15dBZ). This region coincide with that determined as a convective region by the CST.

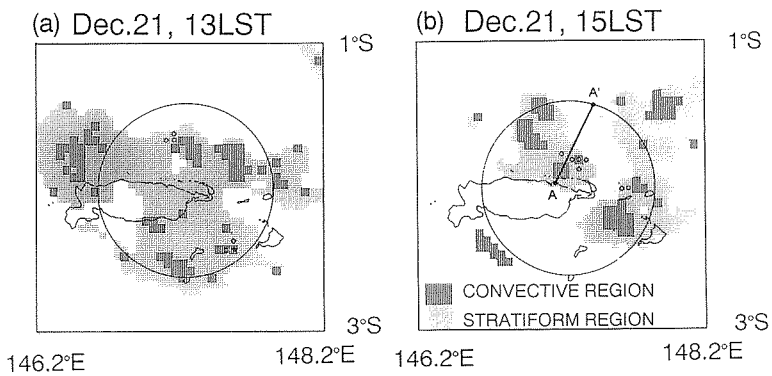

Fig. 11. Same as Fig. 5 except for the time of (a) 13LST and (b) 15LST on December 21, 1992.

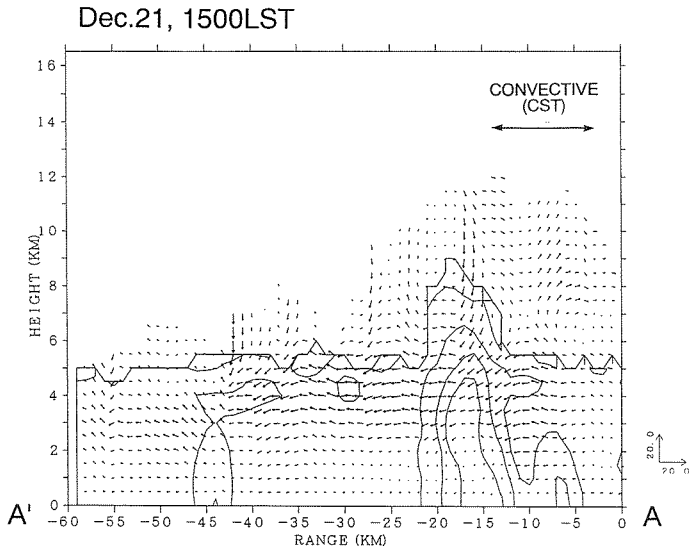

Fig. 12. Vertical cross section along the line A-A′ in Fig. 11, derived from dual-Doppler analysis. Radar reflectivity (dBZ) at 5dBZ intervals from 15dBZ is shown with superimposed with vectors consisted of ground-relative flow and vertical motion. Reflectivity is that of ILTS.

It is thought that this upward motion, which was caused by a different mechanism than that below the melting layer, maintained the thick snow and ice layer in the upper troposphere for a long time. This upward motion was shown in horizontal map as shown in Fig. 10 at the dissipating stage. Similar features are described by Satoh et al. (1995) and Shimizu et al. (1995).

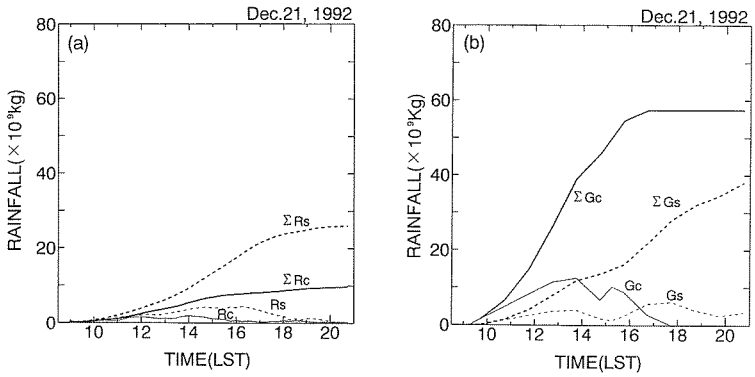

Fig. 13. Same as Fig. 6 except for the day on December 21, 1992.

Next, the area-integrated rain rates and rainfall amounts of the convective and stratiform regions within the radar coverage are shown in Fig. 13 according to the radar echo and the CST as in Case 1. In ths figure, the calculation of convective and stratiform precipitation was carried out in the same way as in Case 1 using the Z-R relationship [Eq. (8)] from PPI (el.=3°) reflectivity data. The curve of the convective rain rate from the radar reached its first peak at 12LST and showed its second peak due to the strong echo below the melting layer at around 14LST, as the radar-derived convective coverage evolved, as in Case 1. The curve of the convective rain rate estimated from the CST shows quite a disagreement with that from the radar, like the relation between the results of the CST and radar echo patterns as shown in Fig. 11. On the other hand, the stratiform rain rate estimated from the radar and CST show relatively good coincidence with each other. Stratiform rain rate reached its maximum at 16LST in the dissipating stage due to a large coverage of stratiform echoes, though that of the CST-derived reached its maximum about an hour later.

The disagreement between the CST and the rader is further shown in the comparison with the total rainfall amounts. Radar data shows the predominance of a stratiform rainfall amount through its life time, the same as was shown in Case 1. However, the CST determined the total convective rainfall to be more than the total stratiform rainfall through its lifetime. Comparing the results between the CST and radar, the CST-derived total convective rainfall amount is estimated to be about six times larger than the amounts of rainfall derived from radar data. It is thought that the overestimation of the area, rain rate and total rainfall of CST-derived convective and stratiform components resulted from a very cold convective cores at about 190°K caused by an overspread thick snow and ice layer.

5. Discussion

In this study, the results of analyses of two characteristic cloud clusters observed during TOGA COARE IOP were presented. In Case 1 (24 November, 1992), a cloud cluster was observed through its lifetime from the developing to the dissipating stage in the radar observation range. Second, a cloud cluster with the expansion of very low T_{BB} region observed on December 21, 1992, in spite of a low echo top height, was described in Case 2. These cases were analyzed using radar and GMS-IR data. Also the CST method was adopted for analyses of GMS-IR data.

In addition to these cases, the same analyses as Case 1 and Case 2 were

made on the case of a sharp line echo (Takahashi and Uyeda, 1995) observed on December 16, 1992. For this case (Case 3), the area-integrated rain rate and rainfall amounts were estimated for the radar and the CST using the same method used in Case 1 and Case 2. However, the data used in this case unfortunately had low resolution of 0.1°. The convective and stratiform area-integrated rain rates and total rainfall amounts were estimated for the radar and the CST using 0.1° resolution data as shown in Fig. 14. In this case, the cloud area of T_{BB} below 220K, corresponding to the cloud top height of 12.5 km, rapidly expanded almost within the whole area of radar coverage in the dissipating stage like Case 2. This rapid increase of the low T_{BB} area was attributed to the expansion of an anvil region associated with the squall line echo. The curve of the convective area-integrated rain rate distinguished from the CST showed rapid increase from 15LST to 17 LST due to the large coverage of the low T_{BB} area. Thick snow and ice layer is presumed because large rainfall rate in convective component was derived from CST and small rainfall amount of convective portion was derived from radar. On the other hand, the total rainfall amounts derived from the radar showed the predominance of stratiform rainfall due to the large coverage of a stratiform region after 1730LST as shown in Fig. 14. In contrast, the CST-derived convective total rainfall amount was about three times larger than the stratiform rainfall amount as shown in Fig. 14. Though it is thought that the rough resolution data used in this case is one of the reasons of the disagreement between the results of the CST and radar, it is considered that the existence of a thick snow and ice layer above the melting layer led to the overestimation of rainfall amount in the same manner as discussed in Case 2.

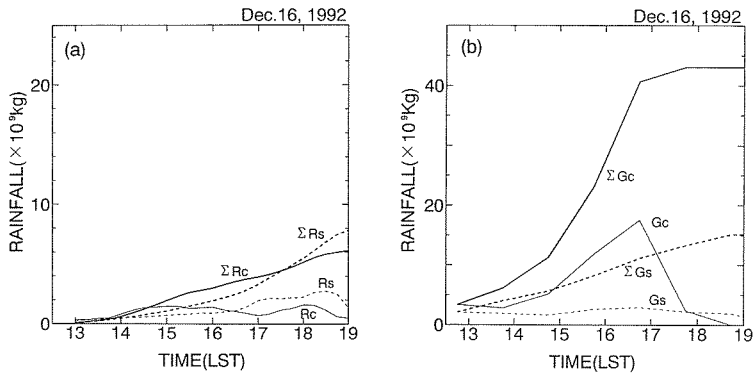

Fig. 14. Same as Fig. 6 except for the day on December 16, 1992.

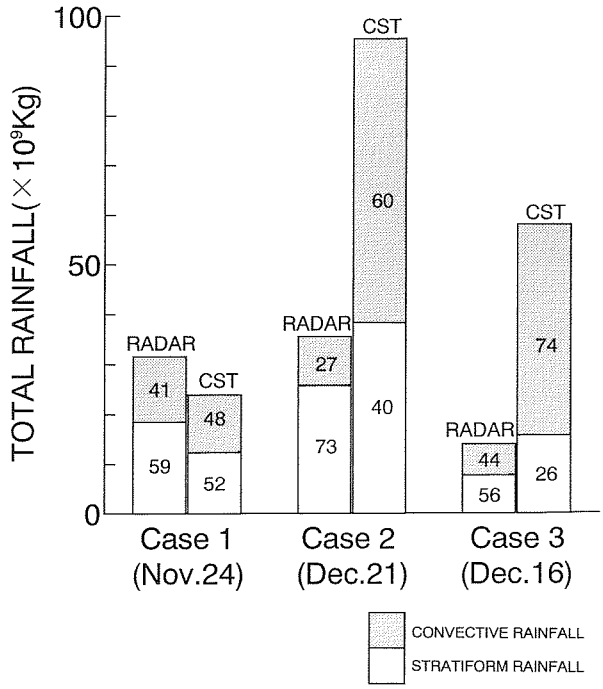

Fig. 15. Stacked column graphs for time-integrated total rainfall amonuts derived from radar and the CST for three cases. Convective and stratiform percentage contributions to the total rainfall amounts are also included. Dark-shaded regions indicate convective contributions.

The ratio between convective and stratiform time-integrated total rainfall amounts derived from the CST and radar data are shown in Fig. 15 for three cases. Stratiform rainfall amounts derived from the radar was larger than that of convective rainfall amounts. Stratiform percentages given by other studies of tropical cloud clusters have ranged from 30 to 50% (Houze, 1977 ; Cheng and Houze, 1979). The value derived from the radar of about 60% (56%-73%) in the present study is much larger than the previous studies. This difference is considered to reflect the thick snow and ice layer of stratiform clouds, lasting for long period, in equatorial western Pacific ocean. On the other hand, the large ratio of convective portion derived from the CST and small ratio of convective portion of radar-derived rainfall amount also implies the existence of convection only above melting layer in thick snow and ice layer.

The distribution of T_{BB} in Case 1 at 13LST and 15LST November 24, in which the best conformance of convective echo area and convective cloud area

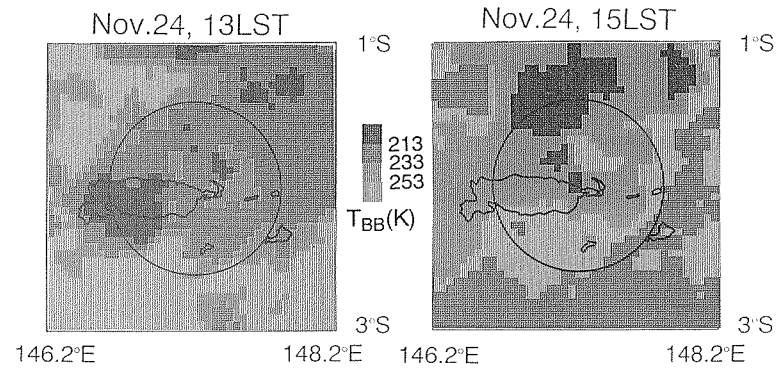

Fig. 16. The distribution of T_{BB} classified by three thresholds on November 24, 1992.

identified with the CST was obtained among three cases, is shown in Fig. 16. The T_{BB} in the radar range is not so low comparing to that of Case 2 and 3. The most part of the T_{BB} is higher than 213K except for the area of high echo top shown in Fig. 5. This enabled us to obtain good conformance between the CST and the radar. On the other hand, the existence of a large coverage of an overspread snow and ice layer in Case 2 is shown in Fig. 17 as the large area of T_{BB} below 213K. In spite of the large coverage of low T_{BB}, Fig. 11 did not show a high radar echo top height. Therefore, the existence of a thick snow and ice layer caused the disagreement in estimating the convective and stratiform components in cloud clusters. Though the analyses of the CST in the present paper suggest the difficulty to determine the rainfall amounts from T_{BB} data only, the effectiveness of the CST analyses in conjunction with Doppler radar

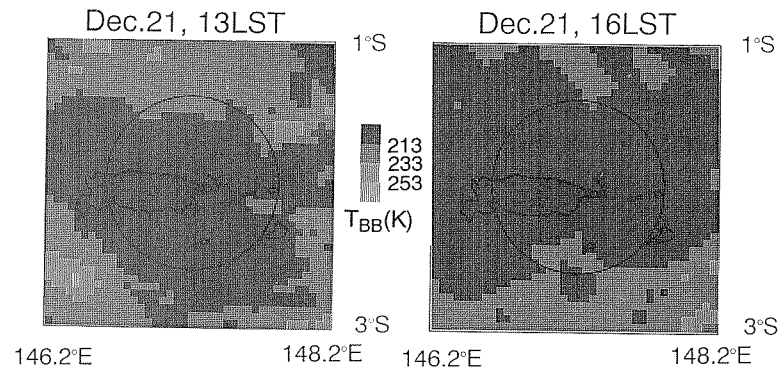

Fig. 17. The distribution of T_{BB} classified by three thresholds on December 21, 1992.

analyses for the study of tropical cloud cluster was confirmed.

In Case 2, it is thought that the cloud cluster had not taken an orographic effect and is regarded as the general cloud cluster over the ocean in tropics. In addition, the distribution of an updraft derived from dual-Doppler analysis shown in Fig. 11 and Fig. 12 indicates a different circulation system between, above and below the melting layer. Similar phenomena are described by Satoh et al. (1995) and Shimizu et al. (1995). The circulation above the melting layer maintained the snow and ice layer for a long time. The existence of the analyzed long lasting thick snow and ice layer above the melting layer may suggest that the radiative influence of snow and ice layer in tropical cloud clusters upon the climate has to be studied in addition to the estimation of rainfall amount.

6. Conclusions

Radar observations of cloud clusters were carried out in Manus Island, Papua New Guinea, from November, 1992 to January, 1993 during TOGA COARE IOP. Of some cloud clusters observed using Doppler radars, two characteristic cloud clusters were chosen for detailed analyses and characteristics of one cloud cluster were compared. From the results of analyses presented, some characteristics of cloud clusters in the equatorial western Pacific ocean were revealed.

Radar data revealed a bimodal distribution of convective rainfall amonut. The first mode consisted of heavy rainfall in the mature stage. The second rainfall corresponded to the relatively weak rainfall below the melting layer within stratiform echoes at the beginning of dissipating stage. However, the results of analyses using radar data also revealed the predominance of a stratiform area and rainfall amounts relative to convective components throughout its lifetime, even in the development to the mature stage.

The analyses of GMS-IRR data were combined with the radar data analyses in order to understand the detailed characteristics of cloud clusters. The comparison between the evolution of the radar echo top height and that of cloud area identified from GMS-IR data, showed the time lag between them. At the same time, the distribution of vertical motion fields derived from dual-Doppler radar analysis showed the time lag between, above and below the melting layer and the maintenance of an updraft above the melting layer ; a low level updraft region is apparent during the developing and the mature stage, and then an upper level updraft region above melting layer predominate and lasted for a long

time after the initiation of dissipating stage. This suggest the existence of a different convective circulation between, above and below the melting layer. It implies that warm rain process predominate at the beginning stage of the cloud development and that the thick snow and ice layer, which was maintained by an updraft above the melting layer, expanded horizontally in the upper troposphere in the dissipating stage of a cloud cluster. This is supported by the comparison between the results of the radar and the results of analyses using the CST, which is the method used to distinguish between convective and stratiform components of cloud clusters. The expansion of a low T_{BB} region caused the difficulty in estimating rainfall amounts from GMS-IR ata though this is one of a characteristics of cloud cluster in this region. In addition, these results suggested the importance to study the characteristics of tropical cloud clusters, which have the expansion of the low T_{BB} region, for understanding the influence of cloud radiation to the climate change.

The results obtained in these analyses using radar and GMS-IR data provided new information on characteristics of cloud clusters in the equatorial western Pacific ocean. It will be helpful for future studies in this region. The successful analyses using radar and satellite data can provide advance understanding and new information on the characteristics and the structures of tropical cloud clusters. In particular, this kind of analysis would be an effective way to reveal the interaction among cloud clusters and furthermore between a cloud cluster and a super cloud cluster, which is regarded as having an important role in the various time-scale variation.

Acknowledgments

The authors would like to express their sincere thanks to Prof. Kikuchi, Dr. Y. Asuma and Dr. N. Takahashi of Hokkaido University for their valuable discussions. And they also express their thanks to Dr. T. Nakazawa of the Meteorological Research Institute for providing high resolution GMS-IR data. They also extend their thanks to Dr. S. Sato of Institute of Low Temperature Science, Hokkaido University, for providing the program and radar data for dual-Doppler analyses. They also thanks members of Manus radar observation group for their support in this observation and many participants of TOGA COARE for providing sounding data and so on. This study was supported by the Grant-in-Aid for Scientific Research from the Ministry of Education, Science and Culture of Japan (No. 06NP021).

References

Adler, R.F. and A.J. Negri, 1988. A satellite infrared technique to estimate tropical convective and stratiform rainfall. J. Appl. Meteor., **27**, 30-51.

Adler, R.F. and R.A. Mack, 1984. Thunderstorm cloud height-rainfall rate relations for use with satellite rainfall estimation techniques. J. Clim. Appl. Meteor., **23**, 280-296.

Cheng, C.-P. and R.A. Houze, Jr., 1979. The distribution of convective and meso-scale precipitation in GATE radar echo patterns. Mon. Wea. Rev., **107**, 1370-1381.

Demaria, M., 1985. Linear response of a stratified tropical atmosphere to convective forcing. J. Atmos. Sci., **42**, 1944-1959.

Goldenberg, S.B., R.A. Houze, Jr. and D.D. Churchill, 1990. Convective and stratiform components of a winter monsoon cloud cluster determined from geosynchronous infrared satellite data. J. Reteor. Soc. Japan, **68**, 37-63.

Hartmann, D.L., H.H. Hendon and R.A. Houze, Jr., 1984. Some implications of the meso-scale circulations in tropical cloud clusters for large-scale dynamics and climate. J. Atmos. Sci., **47**, 2227-2240.

Hayashi, Y.-Y. and A. Sumi, 1986. The 30-40 day oscillations simulated in an "aqua planet" model. J. Meteor. Soc. Japan, **64**, 451-467.

House, Jr., R.A., 1977. Structure and dynamics of a tropical squall-line system. Mon. Wea. Rev., **105**, 1540-1567.

House, Jr., R.A. and A.K. Betts, 1981. Convection in GATE. Geophy. Space Physics, **19**, 541-576.

Marshall, J.S. and W.M. Palmer, 1948. The distribution of raindrops with size. J. Meteor., **5**, 165-166.

Nakazawa, T., 1988. Tropical Super Clusters within Intraseasonal Variations over the Western Pacific. J. Meteor. Soc. Japan, **66**, 823-839.

Ramage, C.S., 1968. Role of a tropical "maritime continent" in the atmospheric circulation. Mon. Wea. Rev., **96**, 365-370.

Satoh, S., A. Kinoshita and H. Uyeda, 1995. Doppler radar observation on the structure and characteristics of tropical clouds during the TOGA-COARE IOP in Manus, Papua New Guinea : Dual-Doppler analysis of meso-scale convective system composing a cloud cluster. J. Meteor. Soc. Japan, **73**, 443-459.

Shimizu, S., H. Uyeda, W. Ecklund and K. Gage, 1995. Doppler radar observation on the structure and characteristics of tropical clouds during the TOGA-COARE IOP in Manus, Papua New Guinea : Fine structure and maintenance of stratiform region of cloud cluster. Dual-Doppler analysis of meso-scale convective system composing a cloud cluster. J. Meteor. Soc. Japan (Submitted).

Takahashi, N. and H. Uyeda, 1995. Doppler radar observations on the structure and characteristics of tropical clouds during the TOGA-COARE IOP in Manus, Papua New Guinea : Three case studies on November 23 and December 16, 1992. J. Meteor. Soc. Japan, **73**, 427-442.

Uyeda, H., Y. Asuma, N. Takahashi, S. Shimizu, O. Kikuchi, A. Kinoshita, S. Matsuoka, M. Katsumata, T. Takeuchi, T. Endo, M. Ohi, S. Satoh, Y. Tachibana, T. Ushiyama, Y. Fujiyoshi, R. Shirooka, N. Nishi, T. Tomita, H. Ueda, T. Sueda, A. Sumi, 1995. Doppler radar observations on the structure and characteristics of tropical clouds during the TOGA-COARE IOP in Manus, Papua New Guinea : Outline of the observation. J. Meteor. Soc. Japan, **73**, 415-426.

World Climate Research Project, 1989. Science Plan for TOGA COARE. WCRP publication (draft), WMO, Geneva, 112 pp.